Performance Evaluation of a Two-Stage Grid-Tied Solar PV System under Multiple Grid Faults using Enhanced LVRT and Harmonic Analysis

Yellu Sharath Reddy[1], Jakkula Sreelatha[2*]
[1]PG Student, [2]Assistant Professor, [1,2]Department of Electrical and Electronics Engineering
[1,2]Vaagdevi College of Engineering (UGC-Autonomous), Bollikunta, Warangal, 506005, Telangana
[1]sharathreddyyellu@gmail.com, [2]Jakkulasreelatha29@gmail.com
*Correspondence: Jakkula Sreelatha (Jakkulasreelatha29@gmail.com)

ABSTRACT
The rapid expansion of renewable energy integration has significantly increased the deployment of grid-connected Solar Photovoltaic (SPV) systems worldwide, with solar energy contributing a major share of newly installed renewable generation capacity each year. Recent energy reports indicate that global photovoltaic installations continue to grow steadily due to increasing electricity demand, environmental concerns, and the transition toward sustainable power generation. Conventional assessment approaches largely depend on manual analysis of voltage, current, and power waveforms under fault conditions, making the evaluation process time-consuming, labour-intensive, and prone to incomplete interpretation. Furthermore, traditional studies primarily focus on limited fault scenarios and often neglect comprehensive harmonic assessment and compliance verification, restricting the overall understanding of inverter performance. To address these limitations, this work presents an Low Voltage Ride Through (LVRT) assessment framework for a two-stage grid-connected SPV system operating under Line-to-Ground (LG), Double-Line-to-Ground (LLG), and Three-Phase-to-Ground (LLLG) fault conditions. The proposed framework employs Maximum Power Point Tracking (MPPT) or Non-MPPT based boost converter control, PI-based DC-link voltage regulation, reactive power oscillation-based reference current generation, and Proportional Resonant (PR) current control for maintaining inverter stability during grid disturbances. In addition, Fast Fourier Transform (FFT) based harmonic analysis, IEEE-519 compliance verification, harmonic compensation mechanisms, and an enhanced LVRT performance evaluation strategy are incorporated to assess voltage recovery, reactive power support, active power regulation, fault ride-through capability, and power quality performance under multiple fault scenarios, thereby providing a comprehensive and reliable assessment of grid-connected photovoltaic system operation.

Keywords: Low Voltage Ride Through (LVRT), Grid-Connected Solar Photovoltaic (SPV), Fault Ride-Through, IEEE-519 Harmonic Analysis, Proportional Resonant (PR) Controller.

1. INTRODUCTION

The rapid growth of renewable energy generation has transformed the structure of modern power systems across the world. Solar photovoltaic (SPV) technology has emerged as one of the most widely adopted renewable energy sources due to its clean operation, low maintenance requirements, and declining installation costs. According to recent global energy reports, solar energy contributes a significant portion of newly installed renewable generation capacity every year, with utility-scale and distributed photovoltaic systems being integrated into residential, commercial, and industrial sectors. Countries such as China, the United States, India, Germany, and Japan continue to expand solar power deployment to meet increasing energy demands while reducing greenhouse gas emissions. The growing penetration of SPV systems has created new challenges for grid operators because photovoltaic generators must remain stable and reliable even during abnormal grid conditions. Unlike conventional power plants that possess large mechanical inertia, solar power systems are highly dependent on power electronic converters, making them more sensitive to voltage disturbances and grid faults.

Modern electric power networks experience various disturbances such as voltage sags, short circuits, line faults, switching transients, and sudden load variations. These disturbances can affect the performance of grid-connected photovoltaic systems and may lead to power quality degradation, reduced energy transfer, and disconnection from the utility grid. International grid codes now require renewable energy systems to remain connected during temporary voltage disturbances and actively support the grid through voltage regulation and reactive power injection. Consequently, maintaining stable operation under fault conditions has become a critical requirement for photovoltaic inverters. The continuous expansion of renewable energy integration, combined with increasing expectations for power quality and grid reliability, has intensified the need for advanced control and assessment strategies capable of ensuring uninterrupted operation during both normal and fault conditions.

Broadly, transmission line faults are categorized into series faults and shunt faults. Series faults, also known as open conductor faults, occur due to the interruption of one or more conductors and are further classified into one open conductor faults and two open conductor faults. Shunt faults, commonly referred to as short-circuit faults, are divided into asymmetrical and symmetrical faults based on the balance of fault currents and voltages. Asymmetrical faults include Line-to-Ground (LG) faults, represented by AG, BG, and CG; Line-to-Line (LL) faults, represented by AB, BC, and CA; and Double-Line-to-Ground (LLG) faults, represented by ABG, BCG, and CAG. These faults create unbalanced operating conditions and are the most frequently occurring faults in practical power systems. Symmetrical faults consist of Three-Phase (LLL) faults, represented by ABC, and Three-Phase-to-Ground (LLLG) faults, represented by ABCG. Although symmetrical faults occur less frequently, they produce the highest fault currents and impose severe stress on power system equipment. This classification provides a comprehensive understanding of fault types and serves as a foundation for analyzing Low Voltage Ride Through (LVRT) performance and power quality behaviour of grid-connected photovoltaic systems under different fault scenarios. The main contributions of this article are as follows:

- To evaluate the Low Voltage Ride Through capability of a two-stage grid-connected Solar Photovoltaic system under LG, LLG, and LLLG fault conditions.
- To analyze the harmonic performance of the injected grid current using FFT-based assessment and verify compliance with IEEE-519 power quality standards.
- To investigate voltage recovery, reactive power support, active power regulation, and overall inverter performance during different grid disturbance scenarios.

2. LITERATURE SURVEY

W. Wan et al. [1] developed a compact and high-precision magnetic encoder aimed at improving sensing performance while reducing device dimensions. The proposed design achieved higher angular resolution by increasing the magnetic pole configuration from two poles to four poles, resulting in nearly double the measurement accuracy compared to conventional structures. Despite these advantages, the method encountered challenges in accurately determining the absolute angular position using traditional detection techniques. S. A. Gopalan et al. [2] presented a comprehensive review of protection coordination approaches and protection schemes designed for microgrids. Their study examined communication-based and time-grading-based coordination methods while discussing their operational characteristics and comparative performance under different fault scenarios. R. Li et al. introduced [3] a fault identification approach for meshed DC networks that distinguishes faulty branches from healthy ones using voltage polarity and magnitude information obtained from DC reactors connected to the same converter terminal. The method enabled rapid fault detection, thereby reducing fault current stress on circuit breakers and converter components. B. Long et al. [4] conducted an extensive review of DC current components in transformer less grid-connected distributed photovoltaic systems. The study discussed the origins of DC current injection, its adverse effects on utility grids, various detection methodologies, and suppression techniques. Furthermore, a comparative analysis of available detection and mitigation approaches was provided.

M. Fan et al. [5] proposed an enhanced grid frequency estimation technique with strong immunity to DC offset disturbances. A four-consecutive-sample (4CS) model was developed to represent the relationship among grid voltage signals, DC offsets, and sampled data. Unlike conventional three-sample models, the proposed framework effectively eliminated the influence of DC offsets and improved frequency estimation accuracy. A. Camacho et al. [6] developed a flexible reference generation strategy capable of maintaining injected current levels within safe operating limits while simultaneously optimizing inverter power utilization. The method enabled coordinated injection of positive and negative active as well as reactive power components to improve fault ride-through performance. H. Khan et al. [7] investigated voltage support mechanisms and current control strategies for photovoltaic systems operating during grid disturbances. The study emphasized coordinated operation between maximum power point tracking and ride-through controllers. In low-voltage networks, active power regulation was prioritized over reactive power support due to lower X/R ratios, while reliable event discrimination ensured stable operation. S.-F. Chou et al. [8] proposed a low-voltage ride-through strategy that maximized converter current utilization while satisfying grid code requirements. The technique effectively controlled converter phase current peaks, compensated transformer flux, and minimized post-fault transformer inrush currents without activating overcurrent protection mechanisms. J. Ge et al. [9] presented a flexible inverter control strategy designed to enhance power injection capability during asymmetrical grid faults. The method incorporated generalized reference current generation with controllable positive, negative, and zero-sequence current components. Additionally, a maximum allowable power injection algorithm was introduced to satisfy peak current and power oscillation constraints.

A. Q. Al-Shetwi et al. [10] proposed a comprehensive LVRT enhancement strategy for single-stage photovoltaic power plants in compliance with modern grid codes and Malaysian standards. The approach employed a DC chopper brake controller to dissipate excess DC-link energy and a current limiter to prevent excessive AC-side currents during fault conditions. G. B. Huka et al. [11] developed a coordinated control framework that incorporated power reference calculation, active power curtailment, inverter peak current limitation, and multiple current reference generation techniques. These strategies collectively improved the reliable operation of photovoltaic systems under various grid fault conditions. E. Afshari et al. [12] introduced a control methodology for two-stage three-phase photovoltaic systems operating under unbalanced grid faults. The study addressed issues such as distorted current injection, active and reactive power oscillations, and double-grid-frequency fluctuations, thereby improving system performance during abnormal operating conditions. K. Shi et al. [13] proposed a virtual synchronous generator control approach in which operation transitions from voltage-source mode to current-source mode during grid faults. The method utilized proportional-resonant current control and phase-angle tracking to facilitate smooth mode switching and reliable reactive power support throughout fault and recovery periods. S. Wang et al. [14] presented an innovative energy storage system control strategy aimed at mitigating photovoltaic power fluctuations while reducing storage capacity requirements. The proposed approach utilized short-term forecasting techniques to enhance compliance with grid regulations and improve storage system utilization efficiency. J. P. Roselyn et al. [15] developed a fuzzy logic-based real and reactive power control scheme for photovoltaic inverters to improve low-voltage ride-through performance. The controller enhanced grid voltage stability through reactive current injection while reducing excessive grid currents by regulating active power delivery.

3. PROPOSED SYSTEM

The proposed system as shown in Figure 2 extends the conventional LVRT strategy of a two-stage grid-connected SPV system by incorporating balanced three-phase-to-ground (LLLG) fault analysis and IEEE-519 based harmonic assessment. The architecture retains the original MPPT/Non-MPPT control mechanism, PI-based DC-link voltage regulation, reference current generation unit, PR controller, and two-level inverter employed in the existing system. In addition to the conventional LG and LLG fault studies, the proposed framework evaluates inverter performance under severe LLLG fault conditions.

Furthermore, FFT-based harmonic analysis and IEEE-519 compliance verification are integrated into the system to assess power quality during fault events. The proposed architecture enables comprehensive analysis of voltage sag mitigation, reactive power support, harmonic distortion reduction, and LVRT capability under multiple fault scenarios.

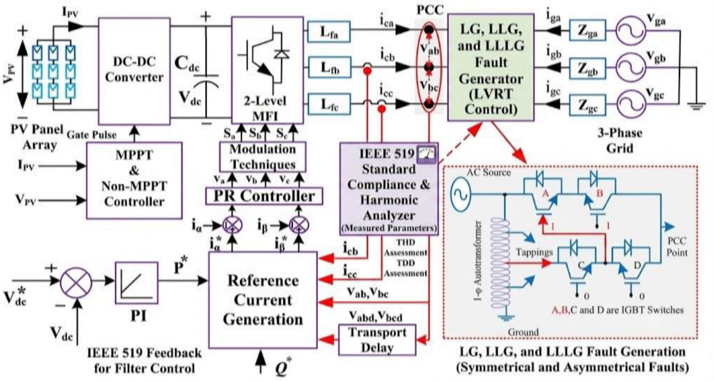

Figure 1. Proposed system control diagram.

Figure 1 shows the flowchart of proposed system. The detailed operation is given as follows:

A. Power Stage Architecture

- **Solar PV Generation:** A photovoltaic array converts solar irradiance and temperature dynamics into DC power, generating variable voltage (V_{pv}) and current (I_{pv}).
- **DC-DC Boost Converter:** Serves as the interface between the PV array and the inverter, stepping up V_{pv} to a regulated DC-link voltage. Under grid faults, it dynamically adjusts its operating point using non-MPPT control to limit active power transfer.
- **DC-Link Capacitor:** Stabilizes the DC bus voltage (V_{dc}), smoothing out voltage ripples and acting as an energy storage buffer between the conversion stages during transient disturbances.
- **Two-Level Voltage Source Inverter (VSI):** Converts the stabilized DC-link power into three-phase AC power. It injects controlled currents into the utility grid via a modulation stage based on grid stability and power quality demands.
- **Filter Inductors:** Line inductors (L_a, L_b, L_c) filter out high-frequency switching harmonics from the VSI output, providing clean sinusoidal currents (I_a, I_b, I_c) to the grid.

B. Control Strategy and Reference Generation

- **Dual-Mode Boost Controller:** Operates in Maximum Power Point Tracking (MPPT) mode during normal grid states. During faults, it automatically switches to a non-MPPT mode to curtail active power extraction, preventing inverter thermal overload while enabling Low-Voltage Ride-Through (LVRT) capability.
- **Outer Voltage Loop:** A Proportional-Integral (PI) controller compares the measured V_{dc} against a reference value to generate the system's active power reference (P^*).
- **Reference Current Generation & Transport Delay:** Processes voltages and currents at the Point of Common Coupling (PCC) alongside P^*. A transport delay block provides delayed voltage signals (V_{d1}, V_{d2}) for sequence component extraction, allowing a reactive power oscillation-based algorithm to compute optimal reference current components (I_d^*, I_q^*).
- **Inner Current Loop & Modulation:** A Proportional Resonant (PR) current controller tracks the generated reference currents to eliminate steady-state errors. Its control outputs are passed to a modulation stage that supplies optimized switching pulses (S_a, S_b, S_c) to the VSI.

C. Fault Injection, Diagnostic Analysis, and Verification

- **Extended Fault Generator:** Evaluates inverter resilience at the PCC under unbalanced Line-to-Ground (LG) and Line-to-Line-to-Ground (LLG) faults, as well as highly severe, balanced Line-to-Line-to-Line-to-Ground (LLLG) faults.

- **Harmonic Analysis & IEEE-519 Compliance:** A FFT module extracts the harmonic spectrum and THD of the grid-injected current. These values are continuously verified against IEEE Standard 519 harmonic limits.
- **LVRT & Performance Assessment:** Evaluates power quality, voltage sag mitigation, active power regulation, and dynamic reactive power injection under all fault states, consolidating these metrics to validate the robustness of the grid-connected solar PV network.

3.1 PROPOSED LVRT CONTROL STRATEGY

The proposed LVRT control strategy is developed for a two-stage grid-connected SPV system to enhance fault tolerance, voltage support capability, and power quality performance under LG, LLG, and LLLG fault conditions. Unlike the existing work that considers only LG and LLG faults, the proposed framework incorporates balanced LLLG fault analysis to evaluate inverter behaviour under the most severe voltage sag scenarios. The system retains the MPPT/Non-MPPT based boost converter control, PI-based DC-link voltage regulation, reactive power oscillation-based reference current generation, and PR current control structure while extending the fault analysis capability. Furthermore, a FFT-based harmonic analysis module and IEEE-519 compliance verification mechanism are integrated into the control architecture. During fault conditions, the controller dynamically regulates active and reactive power references according to voltage sag severity and harmonic distortion levels. The inverter injects the required reactive power to support grid voltage recovery while limiting active power transfer to prevent overcurrent operation. Simultaneously, harmonic distortion of the injected grid current is continuously monitored and utilized to generate a harmonic compensation factor for improving current quality. Consequently, the proposed controller provides enhanced LVRT capability, improved voltage regulation, reduced current harmonics, and compliance with IEEE-519 harmonic standards under LG, LLG, and LLLG fault conditions.

The Clarke transformation as presented in Equation (3,1) converts the measured three-phase PCC voltages from the abcreference frame into the stationary $\alpha\beta$reference frame. This transformation simplifies the analysis of grid disturbances and provides orthogonal voltage components for sequence extraction, power calculation, and reference current generation. The transformed voltages serve as the primary inputs for the proposed LVRT controller.

$$[v_\alpha \; v_\beta] = T_{abc}^{\alpha\beta}[v_a \; v_b \; v_c] \tag{3.1}$$

In this equation, v_a, v_b, and v_c represent the three-phase voltages measured at the PCC. The variables $v_\alpha$and $v_\beta$denote the stationary reference frame voltage components obtained after Clarke transformation, while $T_{abc}^{\alpha\beta}$represents the transformation matrix that converts three-phase quantities into the orthogonal $\alpha\beta$coordinate system.

The positive-sequence voltage magnitude of Equation (3.2) represents the balanced component of the grid voltage and is used to evaluate the healthy operating condition of the utility grid. During normal operation, the positive-sequence voltage remains close to its rated value, whereas fault conditions cause its magnitude to decrease. This parameter is utilized in the proposed controller for determining voltage sag severity and power support requirements.

$$V_{pos} = \sqrt{(v_\alpha^+)^2 + (v_\beta^+)^2} \tag{3.2}$$

Here, V_{pos}denotes the positive-sequence voltage magnitude. The variables $v_\alpha^+$and v_β^+represent the positive-sequence voltage components along the α-axis and β-axis, respectively, obtained from the sequence extraction process.

The negative-sequence voltage magnitude of Equation (3.3) quantifies the level of voltage imbalance introduced by asymmetrical faults such as LG and LLG faults. A larger negative-sequence voltage indicates greater system unbalance and increased power oscillations. This parameter is used for adaptive fault severity assessment within the proposed LVRT strategy.

$$V_{neg} = \sqrt{(v_{\alpha}^{-})^2 + (v_{\beta}^{-})^2} \quad (3.3)$$

In this equation, V_{neg} represents the magnitude of the negative-sequence voltage. The variables v_{α}^{-} and v_{β}^{-} correspond to the negative-sequence voltage components along the α-axis and β-axis, respectively.
The zero-sequence voltage component as denoted in Equation (3.4) is introduced in the proposed framework to analyze grounded fault conditions, especially LLLG faults. It represents the common-mode voltage present in the system and provides additional information regarding fault characteristics. This parameter extends the fault analysis capability beyond the existing LG and LLG fault evaluation.

$$V_{zero} = \frac{|v_a + v_b + v_c|}{3} \quad (3.4)$$

Here, V_{zero} denotes the zero-sequence voltage magnitude, while v_a, v_b, and v_c represent the three-phase PCC voltages used for calculating the average common-mode voltage component.
The per-unit voltage is computed by normalizing the measured voltage magnitude with respect to the nominal system voltage as denoted in Equation (3.5). This normalization enables fault severity assessment independent of the system rating. The calculated value is subsequently used to determine voltage sag intensity and reactive power support requirements.

$$V_{pu} = \frac{\sqrt{v_{\alpha}^2 + v_{\beta}^2}}{V_n} \quad (3.5)$$

In this equation, V_{pu} denotes the per-unit voltage magnitude. The variables v_{α} and v_{β} represent the transformed voltage components in the stationary reference frame, while V_n denotes the nominal grid voltage.
The Voltage Sag Index (VSI) of Equation (3.6) quantifies the depth of voltage reduction experienced during fault conditions. Higher VSI values correspond to more severe voltage sags and consequently require increased reactive power support from the inverter. This index is used by the proposed controller to adapt its LVRT operation according to fault severity.

$$VSI = 1 - V_{pu} \quad (3.6)$$

Here, VSI represents the Voltage Sag Index and V_{pu} denotes the per-unit voltage magnitude calculated from the measured PCC voltages.
The UNP of Equation (3.7) represents the effective inverter power capability available during fault conditions. By incorporating positive-sequence and negative-sequence voltage information, the equation accurately reflects the inverter operating capability under voltage disturbances. The computed value is used to determine power injection limits.

$$UNP = \left(\frac{V_{pos} - V_{neg}}{V_n}\right) S_{inv} \quad (3.7)$$

Here, UNP denotes the Updated Nominal Power of the inverter. The variable S_{inv} represents the apparent power rating of the inverter, V_{pos} denotes the positive-sequence voltage magnitude, V_{neg} represents the negative-sequence voltage magnitude, and V_n indicates the nominal system voltage.
The reactive power reference is dynamically generated according to the measured voltage sag level as shown in Equation (3.8). As the grid voltage decreases, the inverter injects a larger amount of reactive power to support voltage recovery. This adaptive mechanism enhances grid stability and improves LVRT capability.

$$Q_{ref} = S_{inv}(1.5V_{pu}) \quad (3.8)$$

Here, Q_{ref} denotes the reactive power reference generated by the controller. The parameter S_{inv} represents the inverter apparent power rating, while V_{pu} corresponds to the measured per-unit voltage.

Equation (3.9) determines the maximum active power that can be safely delivered by the inverter while maintaining the required reactive power support. Since the inverter has a limited apparent power capability, active power must be reduced whenever reactive power injection increases.

$$P_{max} = \sqrt{UNP^2 - Q_{ref}^2} \quad (3.9)$$

In this equation, P_{max} denotes the maximum allowable active power injection. The variables UNP and Q_{ref} represent the Updated Nominal Power and reactive power reference, respectively.

The THD is calculated using FFT analysis as presented in Equation (3.10) of the injected grid current. It quantifies the amount of harmonic distortion relative to the fundamental current component and serves as a key power quality indicator in the proposed system.

$$THD = \frac{\sqrt{\sum_{n=2}^{N} I_n^2}}{I_1} \times 100 \quad (3.10)$$

Here, THD denotes Total Harmonic Distortion expressed as a percentage. The variable I_1 represents the fundamental current component, I_n denotes the magnitude of the n^{th} harmonic current component, and N indicates the highest harmonic order considered in the analysis.

The Harmonic Compliance Factor presented in Equation (3.11) evaluates the conformity of the measured THD with IEEE-519 harmonic limits. It provides a quantitative measure of power quality performance and enables verification of standard compliance during fault conditions.

$$HCF = 1 - \frac{THD}{THD_{IEEE}} \quad (3.11)$$

In this equation, HCF denotes the Harmonic Compliance Factor. The variable THD represents the measured Total Harmonic Distortion, while THD_{IEEE} denotes the maximum permissible THD limit specified by IEEE-519. The Harmonic Compensation Factor presented in Equation (3.12) adjusts controller operation according to the measured harmonic distortion level. As harmonic distortion increases, the compensation factor decreases, thereby reducing current stress and improving waveform quality.

$$K_h = \frac{1}{1+THD} \quad (3.12)$$

Here, K_h denotes the Harmonic Compensation Factor and THD represents the measured Total Harmonic Distortion of the injected grid current.

The active power reference is modified according to Equation (3.13) using the harmonic compensation factor to ensure both fault ride-through capability and power quality improvement. This adaptive strategy allows the inverter to operate safely during severe fault conditions.

$$P_{ref} = K_h \times P_{max} \quad (3.13)$$

In this equation, P_{ref} denotes the enhanced active power reference, K_h represents the harmonic compensation factor, and P_{max} corresponds to the maximum allowable active power.

Equation (3.14) generates the α-axis reference current by combining active power control, reactive power support, and harmonic compensation. The generated current component is used by the PR controller to regulate inverter operation and improve LVRT performance.

$$i_\alpha^* = K_h \left(\frac{P_{ref}v_\alpha + Q_{ref}v_\beta}{v_\alpha^2 + v_\beta^2}\right) \quad (3.14)$$

Here, i_α^* represents the α-axis reference current. The variables P_{ref} and Q_{ref} denote the active and reactive power references, respectively, while K_h represents the harmonic compensation factor and v_α, v_β denote stationary reference frame voltages.

The β-axis reference current complements the α-axis reference current and together they form the complete current reference vector as denoted in Equation (3.15). This formulation ensures balanced current injection, reduced harmonic distortion, and effective voltage support during fault conditions.

$$i_\beta^* = K_h \left(\frac{P_{ref} v_\beta - Q_{ref} v_\alpha}{v_\alpha^2 + v_\beta^2} \right) \quad (3.15)$$

In this equation, i_β^* denotes the β-axis reference current. The variables P_{ref}, Q_{ref}, K_h, v_α, and v_β retain their previously defined meanings.

The proposed LVRT Performance Index presented in Equation (3.16) provides a unified measure of voltage recovery performance and harmonic compliance during fault conditions. It enables quantitative comparison of controller performance under LG, LLG, and LLLG faults. A higher index value indicates superior ride-through capability and better power quality performance.

$$LVRT_{PI} = \frac{V_{rec} \times HCF}{VSI + \epsilon} \quad (3.16)$$

Here, $LVRT_{PI}$ denotes the LVRT Performance Index, V_{rec} represents the voltage recovery ratio, HCF denotes the Harmonic Compliance Factor, VSI corresponds to the Voltage Sag Index, and ε represents all positive constant introduced to avoid division-by-zero conditions.

4. SIMULATION RESULTS

Figure 2 illustrates the complete MATLAB/Simulink implementation of the proposed two-stage grid-connected solar photovoltaic system integrated with LVRT functionality. The model consists of a photovoltaic array operating at an irradiance of approximately 1000 W/m² and a temperature of 25°C, a DC–DC boost converter, DC-link capacitor, three-phase voltage source inverter, filter network, utility grid, load, and fault generation subsystem. The DC-link voltage is regulated around 250 V, while the inverter converts the harvested solar power into balanced three-phase AC power. The simulation framework enables the analysis of LG, LLG, and LLLG fault conditions, voltage support capability, reactive power injection, power transfer characteristics, and harmonic performance under grid disturbances.

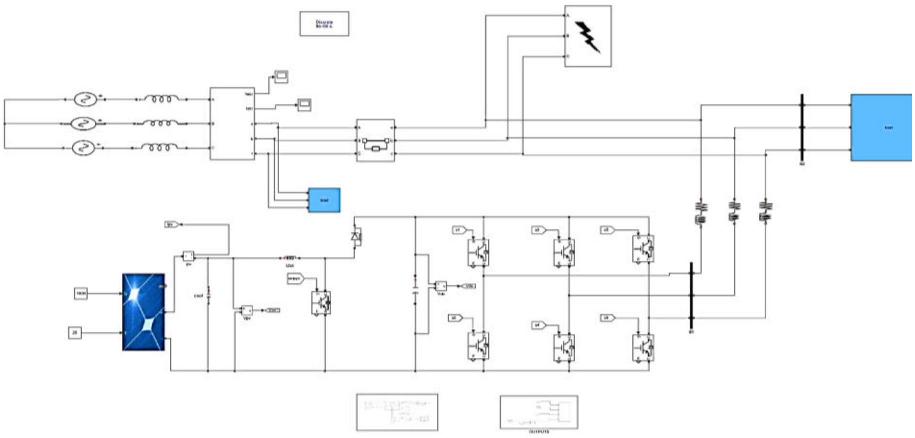

Figure 2. Simulation model of the proposed grid-connected SPV system with LVRT capability.

4.1 SIMULATION ANALYSIS BEFORE FAULT OCCURRENCE

Prior to fault initiation, both the three-phase grid voltage (Figures 3) and inverter current (Figure 4) operate under optimal, balanced conditions at a steady 50 Hz with a strict 120° phase separation. The voltage maintains a stable peak amplitude of ±97 V (0 to 0.1 s), while the injected current remains distortion-free with a peak amplitude of ±80 A (0 to 0.095 s). These clean, symmetrical waveforms confirm precise synchronization between the inverter and the utility grid, validating the high-quality power flow regulation and steady-state effectiveness of the integrated MPPT, PI, and PR control strategies before any disturbance.

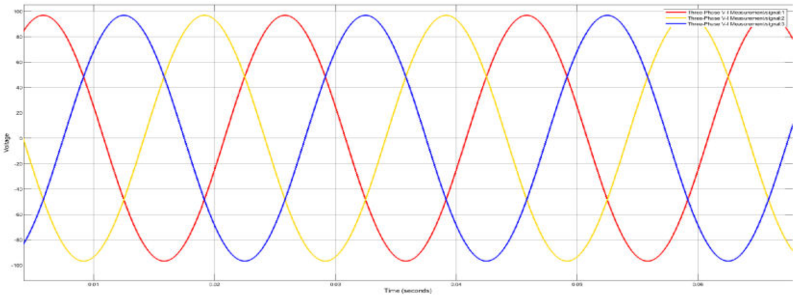

Figure 3. Three-phase grid voltage waveforms before fault occurrence.

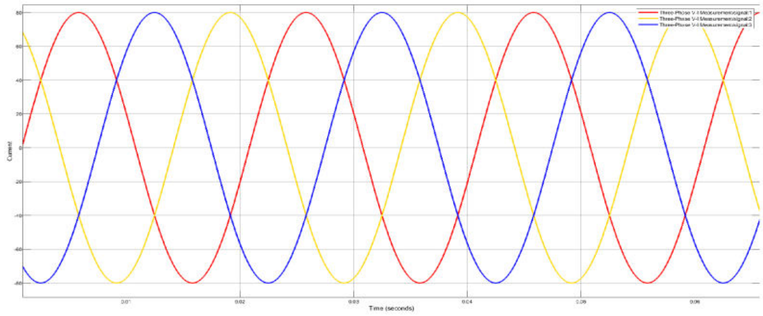

Figure 4. Three-phase grid current waveforms before fault occurrence.

4.2 SIMULATION ANALYSIS AFTER L-G FAULT OCCURRENCE

During a Line-to-Ground (L-G) fault, the affected phase voltage drops from its ± 97 Vpre-fault peak to nearly ± 73 V, while the healthy phases maintain amplitudes close to ± 91 V (Figure 5). Despite this asymmetrical voltage sag, the proposed Low-Voltage Ride-Through (LVRT) controller preserves a stable 50 Hz operating frequency and keeps all three voltage waveforms smooth, sinusoidal, and free of severe oscillations. Concurrently, Figure 6 shows that the inverter current is effectively regulated by the proportional-resonant (PR) control scheme, yielding smooth, distortion-free current transitions. The system limits the peak current to ± 60 Ain the faulted phase and ± 76 Ain the healthy phases. This controlled performance confirms that the inverter maintains precise grid synchronization and continues supplying reliable current, providing necessary fault ride-through support and reactive power compensation throughout the disturbance window.

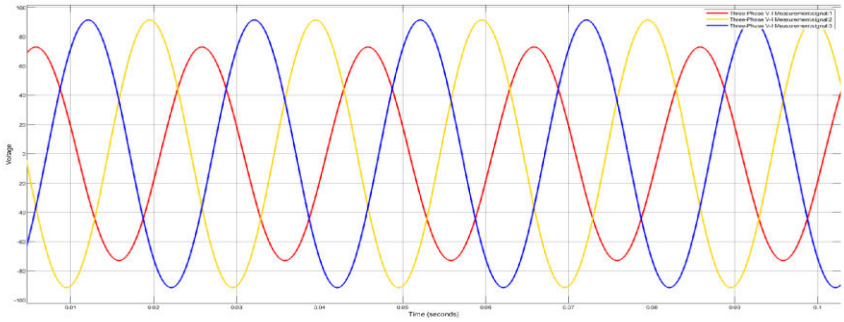

Figure 5. Three-phase grid voltage waveforms after L-G fault occurrence.

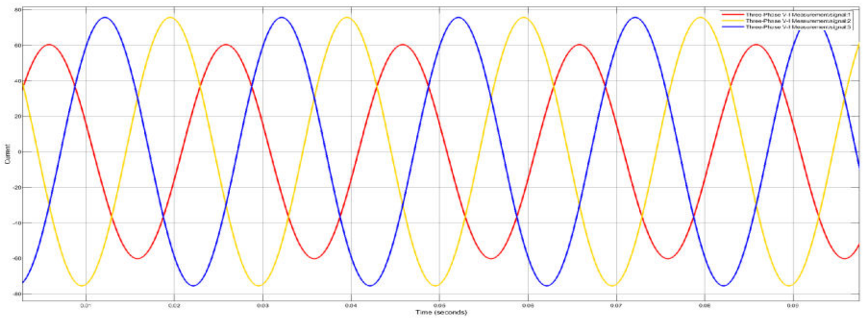

Figure 6. Three-phase grid current waveforms after L-G fault occurrence.

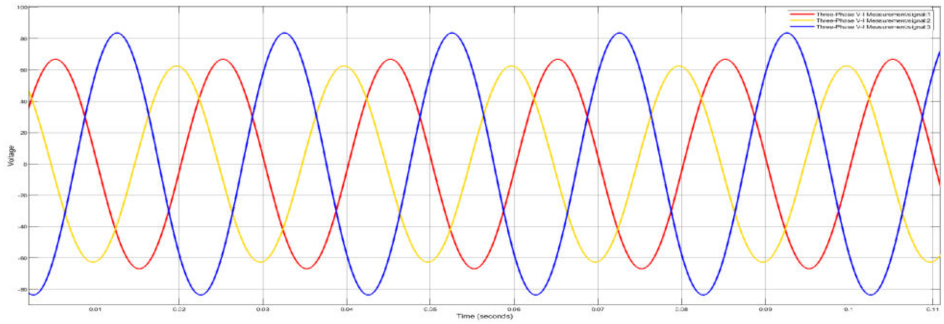

Figure 7. Three-phase grid voltage waveforms after L-L-G fault occurrence.

4.3 SIMULATION ANALYSIS AFTER L-L-G FAULT OCCURRENCE

During a Double-Line-to-Ground (L-L-G) fault, the grid voltage profile becomes highly unbalanced, with the red and yellow phase voltages sagging to peaks of ± 67 Vand ± 62 V, respectively, while the healthy blue phase drops to ± 83 V (Figure 7). Despite this severe asymmetrical disturbance, the proposed LVRT controller maintains a stable 50 Hz nominal frequency and preserves smooth, sinusoidal voltage characteristics to prevent voltage collapse. Simultaneously, Figure 8 reveals that the inverter current redistributes cleanly without excessive oscillations or distortion, yielding regulated peak values of ± 55 A (red phase), ± 51 A (yellow phase), and ± 69 A (blue phase). This highly stable performance demonstrates that the PR controller successfully manages current injection, ensuring the photovoltaic inverter remains securely synchronized with the grid to provide essential reactive power support and robust fault ride-through functionality throughout the L-L-G event.

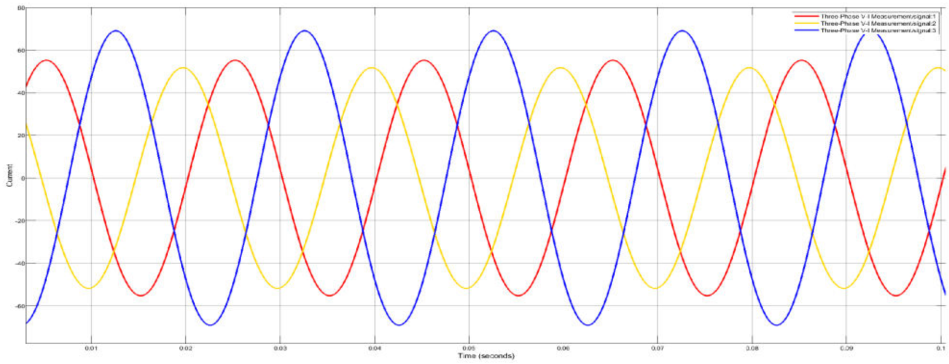

Figure 8. Three-phase grid current waveforms after L-L-G fault occurrence.

4.4 SIMULATION ANALYSIS AFTER L-L-L-G FAULT OCCURRENCE

During a symmetrical Three-Phase-to-Ground (L-L-L-G) fault, all three grid voltages experience a substantial, balanced reduction from their ± 97 Vpre-fault value, dropping to peak magnitudes of ± 57 V (red), ± 53 V (yellow), and ± 48 V (Figure 9). Despite this severe voltage sag, the proposed LVRT controller successfully preserves waveform symmetry, stabilizes the system at a nominal 50 Hz, and prevents voltage collapse. Concurrently, Figure 10 shows that the inverter current magnitudes are symmetrically reduced and tightly regulated to peak values of ± 47 A (red), ± 44 A (yellow), and ± 40 A. The current waveforms maintain a smooth, sinusoidal profile at 50 Hz without severe oscillations or distortion. This balanced response validates the effectiveness of the PR controller and PWM strategy, proving the system can maintain stable current injection and secure grid connectivity under severe three-phase faults.

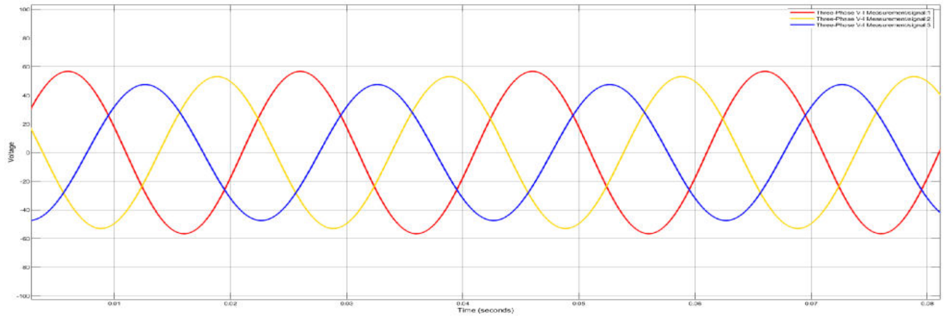

Figure 9. Three-phase grid voltage waveforms after L-L-L-G fault occurrence.

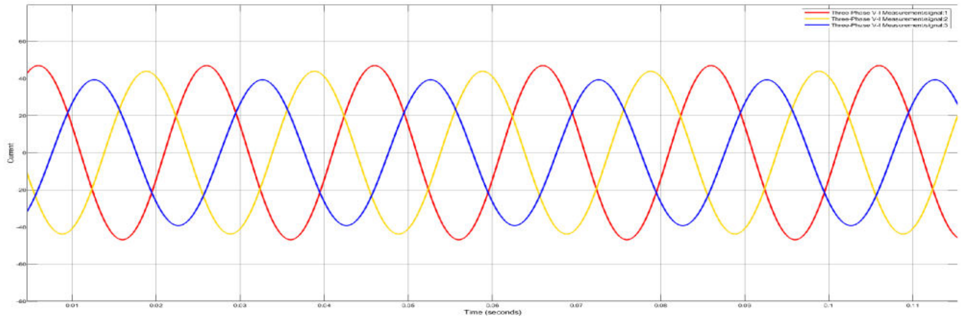

Figure 10. Three-phase grid current waveforms after L-L-L-G fault occurrence.

4.5 OUTPUT SIMULATION ANALYSIS

Throughout the simulation interval (0–0.5 s), Figure 11 demonstrates that the three-phase load voltages remain completely balanced and sinusoidal at a stable peak magnitude of ± 130 Vwith a strict 120° phase separation. Despite external grid disturbances, the proposed LVRT strategy successfully prevents voltage sags, distortion, or severe oscillations at the load terminals, ensuring uninterrupted power quality. Simultaneously, Figure 12 shows that the delivered load currents are perfectly balanced and sinusoidal, maintaining stable peak values of ± 9.5 Aat a nominal 50 Hz frequency. These distortion-free waveforms feature smooth transitions and uniform phase distribution, confirming that the PR current controller and PWM switching strategy effectively regulate the inverter output. Together, these results verify robust load voltage regulation and highly reliable, continuous power delivery under both normal and fault conditions. Throughout the simulation period (0–0.5 s), Figure 13 demonstrates that the DC-link voltage is tightly maintained at a nearly constant 250 V with negligible voltage ripple. This highly stable profile confirms the effective regulation of the PI controller and seamless energy balance coordination between the photovoltaic source, boost converter, and inverter stages, preventing harmful overvoltages during grid disturbances. Simultaneously, Figure 21 illustrates the inverter's output power profile, which initially ramps from 1800 W to nearly 4000 W within the first 0.05 s to reach its operating point. Driven by active power limitation and LVRT control actions during the fault ride-through window, the power gradually drops to 2650 W at 0.45 s and further reduces to nearly 1100 W by 0.5 s. Despite these reductions, the controller successfully manages the power flow, ensuring the inverter continuously injects controlled power while sustaining grid connectivity and system stability.

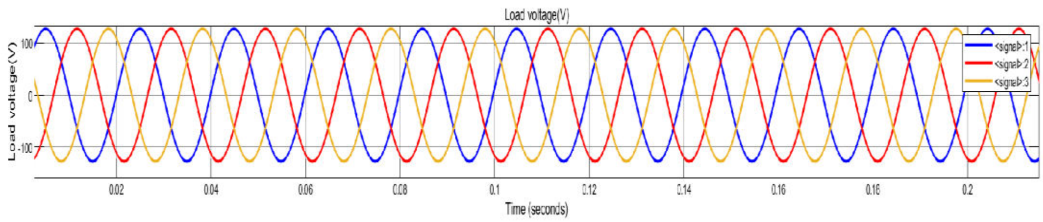

Figure 11. Three-phase load voltage waveforms of the proposed LVRT-controlled SPV system.

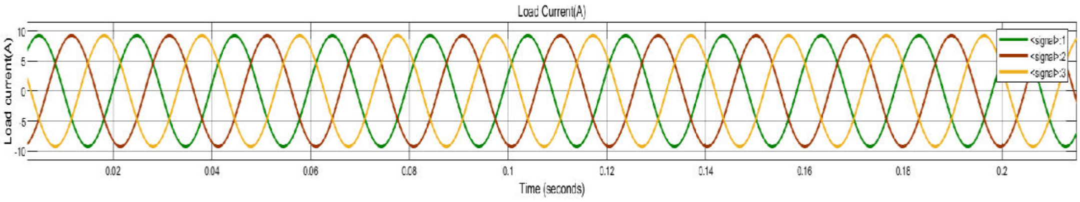

Figure 12. Three-phase load current waveforms of the proposed LVRT-controlled SPV system.

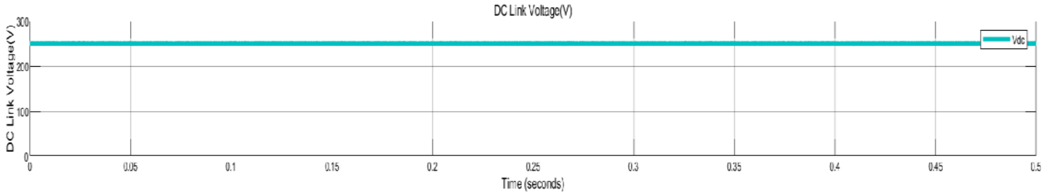

Figure 13. DC-Link voltage response of the proposed LVRT-controlled SPV system.

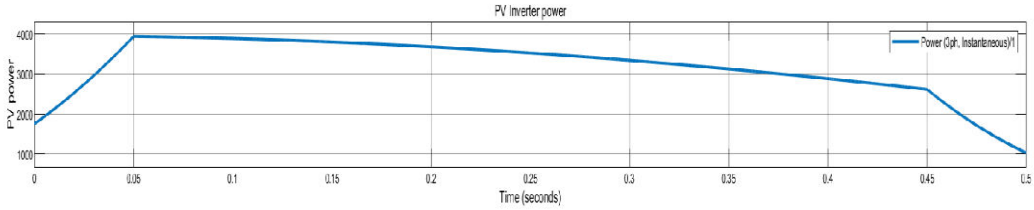

Figure 14. PV inverter output power characteristics during LVRT operation.

4.6 THD ANALYSIS

As listed in Table 1, across all analyzed asymmetrical and symmetrical fault conditions (L-G, L-L-G, and L-L-L-G), the system consistently maintains a stable 50 Hz fundamental operating frequency, with fundamental magnitudes scaling tightly between 125.7 V to 126.7 V for grid voltage and 9.088 A to 9.189 A for inverter current. The data reveals an inverse relationship between fault severity and harmonic distortion: the single line-to-ground (L-G) fault experiences the highest distortion levels due to asymmetrical imbalances and transient reactive power injection—peaking current THD at 5.78%—whereas the most severe balanced symmetrical fault (L-L-L-G) yields the cleanest metrics, achieving an exceptional voltage THD of just 0.78% and a current THD of 1.90%.

Table 1: Comprehensive FFT and THD performance comparison across fault conditions.

Fault Type	Measured Variable	Frequency (Hz)	Magnitude	Measured THD (%)	Control Strategy Performance / Quality
L-G Fault	Grid Voltage	50	125.7 V	3.82%	Acceptable limits; low magnitudes up to 1000 Hz
	Inverter Current	50	9.088 A	5.78%	Inverter reactive power support distortion; limited by PR controller
	Grid Voltage	50	126.6 V	1.15%	Excellent voltage quality;

L-L-G Fault					effective harmonic suppression
	Inverter Current	50	9.159 A	3.05%	Improved waveform quality over L-G fault; effectively regulated
L-L-L-G Fault	Grid Voltage	50	126.7 V	0.78%	Lowest voltage THD; highly preserved waveform quality
	Inverter Current	50	9.189 A	1.90%	Superior current quality; well below the 5% IEEE-519 limit

Ultimately, this consolidated dataset demonstrates the high efficacy of the proposed LVRT framework, PR current controller, and PWM modulation strategy in successfully mitigating fault-induced distortion, keeping the highly critical three-phase current profiles well below the strict 5% limit dictated by the IEEE-519 standard, and guaranteeing superior power quality and grid stability.

5. CONCLUSION

This work successfully developed an LVRT assessment framework for a two-stage grid-connected SPV system by enhancing the conventional LVRT strategy with additional fault and power quality evaluation capabilities. Compared with the existing LVRT framework, which is limited to LG and LLG fault analysis, the proposed system incorporates comprehensive LLLG fault assessment, thereby providing a more complete evaluation of inverter performance under severe symmetrical and asymmetrical grid disturbances. The integration of FFT-based harmonic analysis, IEEE-519 compliance verification, harmonic compensation assessment, and an LVRT performance evaluation framework significantly improve the system's analytical capability. The proposed approach effectively maintains stable load voltage, balanced current injection, regulated DC-link voltage, and reliable power transfer during fault conditions. Future work can focus on extending the proposed LVRT framework to multi-level inverter topologies and hybrid renewable energy systems incorporating wind and energy storage units. Advanced intelligent controllers based on Artificial Intelligence, Deep Learning, or Adaptive Control techniques can be integrated to further improve fault response and dynamic performance.

REFERENCES

[1] W. Wan, et al., "Active fault management for microgrids," In IECON 2018-44th Annual Conference of the IEEE Industrial Electronics Society, pp. 3815–3820. IEEE, 2018.

[2] S. A. Gopalan, V. Sreeram and H. H. Iu, "A review of coordination strategies and protection schemes for micro grids," Renew. Sustain. Energy Rev., vol. 32, pp. 222–228, 2014. DOI: 10.1016/j.rser.2014.01.037.

[3] R. Li, L. Xu and L. Yao, "Dc fault detection and location in meshed multiterminal hvdc systems based on dc reactor voltage change rate," IEEE Trans. Power Deliv., vol. 32, no. 3, pp. 1516–1526, 2017. DOI: 10.1109/TPWRD.2016. 2590501.

[4] B. Long, M. Zhang, Y. Liao, L. Huang and K. T. Chong, "An overview of dc component generation, detection and suppression for grid-connected converter systems," IEEE Access, vol. 7, pp. 110426–110438, 2019. DOI: 10.1109/ ACCESS.2019.2934175.

[5] M. Fan, Z. Dai, Y. Yang, M. Xie, L. He and G. Du, "Four consecutive samples based frequency estimation for single phase grids with dc offsets," IEEE Trans. Ind. Electron, vol. 68, no. 10, pp. 9598–9606, 2021. DOI: 10.1109/TIE.2020. 3028805.

[6] A. Camacho, M. Castilla, J. Miret, A. Borrell and L. G. d. Vicu~na, "Active and reactive power strategies with peak current limitation for distributed generation inverters during unbalanced grid faults," IEEE Trans. Ind. Electron, vol. 62, no. 3, pp. 1515–1525, 2015. DOI: 10.1109/TIE.2014. 2347266.

[7] H. Khan, S. J. Chacko, B. G. Fernandes and A. Kulkarni, "Reliable and effective ride-through controller operation for smart pv systems connected to lv distribution grid under abnormal voltages," IEEE J. Emerg. Sel. Topics Power Electron, vol. 8, no. 3, pp. 2371–2384, 2020. DOI: 10.1109/ JESTPE.2019.2918620.

[8] S.-F. Chou, C.-T. Lee, H.-C. Ko and P.-T. Cheng, "A low voltage ride-through method with transformer flux compensation capability of renewable power grid-side converters," IEEE Trans. Power Electron, vol. 29, no. 4, pp. 1710–1719, 2014. DOI: 10.1109/TPEL.2013.2266511.

[9] J. Ge, Z. Shuai, C. Tu, A. Luo and Z. J. Shen, "Flexible control strategy for enhancing power injection capability of three-phase four-wire inverter during asymmetrical grid faults," IEEE Trans. Power Electron, vol. 36, no. 8, pp. 9592–9608, 2021. DOI: 10.1109/TPEL.2021.3054827.

[10] A. Q. Al-Shetwi, M. Z. Sujod and F. Blaabjerg, "Low volt age ride-through capability control for single-stage inverter based grid-connected photovoltaic power plant," Solar Energy, vol. 159, pp. 665–681, 2018. DOI: 10.1016/j.sol ener.2017.11.027.

[11] G. B. Huka, W. Li, P. Chao and S. Peng, "A comprehensive lvrt strategy of two-stage photovoltaic systems under bal anced and unbalanced faults," Int. J. Elect. Power Energy Syst., vol. 103, pp. 288–301, 2018. DOI: 10.1016/j.ijepes. 2018.06.014.

[12] E. Afshari, B. Farhangi, Y. Yang and S. Farhangi, A low voltage ride-through control strategy for three-phase grid connected pv systems. In 2017 IEEE Power and Energy Conference at Illinois (PECI), pages 1–6. IEEE, 2017. DOI: 10.1109/PECI.2017.7935767.

[13] K. Shi, W. Song, P. Xu, R. Liu, Z. Fang and Y. Ji, "Low voltage ride-through control strategy for a virtual synchron ous generator based on smooth switching," IEEE Access, vol. 6, pp. 2703–2711, 2018. DOI: 10.1109/ACCESS.2017. 2784846.

[14] S. Wang and X. Li, Low Voltage Ride through Control of Cascaded Inverter for Grid-Connected Photovoltaic Systems under Asymmetric Grid Fault Conditions. In IECON 2017 43rd Annual Conference of the IEEE Industrial Electronics Society, pp. 2563–2569. IEEE, 2017.

[15] J. P. Roselyn, et al., "Design and implementation of fuzzy logic based modified real-reactive power control of inverter for low voltage ride through enhancement in grid connected solar pv system," Control Engineering Practice, vol. 101, pp. 104494, 2020. DOI: 10.1016/j.conengprac.2020.104494.